

# Highly Sensitive Detection of Polarized Light Using Anisotropic 2D ReS<sub>2</sub>

Fucai Liu, Shoujun Zheng, Xuexia He,\* Apoorva Chaturvedi, Junfeng He, Wai Leong Chow, Thomas R. Mion, Xingli Wang, Jiadong Zhou, Qundong Fu, Hong Jin Fan, Beng Kang Tay, Li Song, Rui-Hua He, Christian Kloc, Pulickel M. Ajayan, and Zheng Liu\*

Due to the novel optical and optoelectronic properties, 2D materials have received increasing interests for optoelectronics applications. Discovering new properties and functionalities of 2D materials is challenging yet promising. Here broadband polarization sensitive photodetectors based on few layer ReS<sub>2</sub> are demonstrated. The transistor based on few layer ReS<sub>2</sub> shows an n-type behavior with the mobility of about 40 cm<sup>2</sup> V<sup>-1</sup> s<sup>-1</sup> and on/off ratio of 10<sup>5</sup>. The polarization dependence of photoresponse is ascribed to the unique anisotropic in-plane crystal structure, consistent with the optical absorption anisotropy. The linear dichroic photodetection with a high photoresponsivity reported here demonstrates a route to exploit the intrinsic anisotropy of 2D materials and the possibility to open up new ways for the applications of 2D materials for light polarization detection.

communication, near field imaging, remote sensing, as well as to military applications.<sup>[1]</sup> It demands the capability of high detection sensitivity yet compactness for achieving a high level of integration and flexibility. By far, devices commercially available are incapable of meeting these requirements. Most technological implementations integrate the detection component with polarization element in a nonmonolithic platform. In addition, a flexibly integrated device will enable a better adaptability of the polarized optical system, while classic quantum-well based photodetectors, which utilizes a grating to couple the incident light into the quantum wells, are not suitable to flexible applica-

## 1. Introduction

Light polarization is an important concept in optics, discussing the generation, detection, and manipulation of light with certain vibration direction and period. Detection of light polarization has been adapted to various fields, ranging from

tions.<sup>[2]</sup> In order to examine the direction of polarization in an efficient and convenient way, certain materials like nanowire or carbon nanotube have been proposed because of their intrinsically high sensitivity and flexibility.<sup>[3,4]</sup> However, these materials require sophisticated technologies to pattern the devices and align channel materials. The emerging 2D materials such

Dr. F. Liu, Dr. X. He, A. Chaturvedi, J. Zhou, Q. Fu, Prof. C. Kloc  
School of Materials Science and Engineering  
Nanyang Technological University  
Singapore 639798, Singapore  
E-mail: xhe@ntu.edu.sg

S. Zheng, Dr. H. J. Fan  
Centre for Disruptive Photonic Technologies  
School of Physics and Mathematics Sciences  
Nanyang Technological University  
Singapore 637371, Singapore

Dr. J. He, T. R. Mion, Dr. R.-H. He  
Department of Physics  
Boston College  
Chestnut Hill, MA 02467, USA

W. L. Chow, X. Wang, Dr. Z. Liu, Prof. B. K. Tay  
NOVITAS, Centre for Micro-/Nano-electronics  
School of Electrical and Electronic Engineering  
Nanyang Technological University  
Singapore 639798, Singapore  
E-mail: z.liu@ntu.edu.sg

W. L. Chow, Prof. B. K. Tay, Dr. Z. Liu  
CINTRA CNRS/NTU/THALES  
UMI 3288  
Research Techno Plaza  
50 Nanyang Drive, Border X Block  
Level 6, Singapore 637553, Singapore

Prof. L. Song  
National Synchrotron Radiation Laboratory  
University of Science and Technology of China  
Hefei, Anhui 230026, P. R. China

Prof. P. M. Ajayan  
Department of Materials Science and Nanoengineering  
Rice University  
Houston, TX 77005, USA

Dr. Z. Liu  
Center for Programmable Materials  
School of Materials Science and Engineering  
Nanyang Technological University  
Singapore 639798, Singapore



DOI: 10.1002/adfm.201504546

as graphene and MoS<sub>2</sub> shed a light to the detection of polarization due to their unique crystal structures and high sensitivity to the light.

When materials are scaled to 2D, or even to monolayer limit, they exhibit unique properties and phenomena which are distinct from their bulk counterparts. This emerges primarily due to the quantum confinement effect.<sup>[5–9]</sup> For example, room temperature quantum Hall effect has been observed in graphene.<sup>[10–12]</sup> From the aspect of optical behaviors, an indirect to direct band crossover, valley-selective circular dichroism, and large exciton binding energy showed up in transition metal dichalcogenides (TMDs) like MoS<sub>2</sub> and WS<sub>2</sub>.<sup>[13–17]</sup> Though a very promising candidate, there are few reports on the detection of polarized light using 2D materials.<sup>[18–20]</sup> ReS<sub>2</sub> is a typical layered TMD with a band gap of 1.5 eV. It has distorted 1T highly-anisotropic in-plane structure which will induce electrons and photons with anisotropic nature within the layer plane.<sup>[21,22]</sup> In addition, ReS<sub>2</sub> has been reported to have vanishing interlayer coupling,<sup>[23]</sup> and integrated inverter based on the conductivity anisotropy of ReS<sub>2</sub> has been demonstrated.<sup>[24]</sup> ReS<sub>2</sub> has also been used as a platform for the study of ballistic transport.<sup>[25]</sup> These unique properties of ReS<sub>2</sub> may enable a new research field of electronics and photonics device where the strong anisotropic properties of 2D materials can be used to design conceptually novel electronic and optoelectronic device applications. In this article, a polarization sensitive photodetector with high photoresponsivity is demonstrated based on atomically thin ReS<sub>2</sub>, benefiting from the anisotropic nature of the material itself. It is completely different from existing photodetectors for polarization sensitive detection which requires the use of extra components such as gratings to couple the incident light.<sup>[26]</sup> Our study shows that atomically thin ReS<sub>2</sub> may pave a promising way to the applications on the integrated photonic circuits, optical switches, and interconnects for detecting the various orientations of linearly polarized light in a highly integrated photonic platform.

## 2. Characterization of ReS<sub>2</sub> Flakes

Similar to the layered structure of other TMDs, ReS<sub>2</sub> crystallizes in a lattice with strong covalent in-plane bonds and weak van der Waals interlayer interactions (Figure 1a, side view of ReS<sub>2</sub>). Such strong anisotropy from the asymmetric structure bonds leads to many anisotropic behaviors, such as their electrical and optical property difference between the directions parallel and perpendicular to the layers. Besides, the distorted CdCl<sub>2</sub> layer structure of ReS<sub>2</sub> leads to triclinic symmetry and large in-plane anisotropy,<sup>[27]</sup> which is significantly different from other TMDs with hexagonal structures like MoS<sub>2</sub>. Figure 1b shows the top view of ReS<sub>2</sub> crystal structure. We can see that Peierls distortion of the 1T structure results in buckled S layers

and zigzag Re chains along one of the lattice vectors (*b*-axis) in the plane. The intrinsic anisotropy of ReS<sub>2</sub> provides a new degree of freedom to manipulate its optical and optoelectronic properties for novel integrated device applications.

To investigate the optical and electrical properties of the ReS<sub>2</sub> atomically thin flakes, a scotch tape based mechanical exfoliation method was used to peel thin flakes from bulk crystal onto degenerately doped silicon wafer covered with 285 nm SiO<sub>2</sub>.<sup>[28]</sup> The morphology and thickness of the exfoliated ReS<sub>2</sub> were characterized by optical microscopy, high resolution transmission electron microscopy (HRTEM), and atomic force microscopy (AFM), respectively. Figure 1c,d shows the HRTEM images and corresponding fast Fourier transform (FFT) pattern taken from few layer ReS<sub>2</sub> flake, confirming high crystallinity of the exfoliated ReS<sub>2</sub>. The distortion of Re atom arrangement from perfect hexagonal symmetry creates a distortion of the S atom arrangement in the layer plane. The Re chains formed by distortion is clearly seen in the TEM image along the *b*-axis. The structural anisotropy leads to orientation-dependent electric and optical properties, which will be discussed in details below. Figure 2a shows the typical optical image of ReS<sub>2</sub> thin flake on SiO<sub>2</sub> substrate. The AFM image of the ReS<sub>2</sub> flake is shown in Figure 2b. The monolayer ReS<sub>2</sub> can be identified from the line profile displayed in Figure 2c. Figure 2d shows the Raman spectrum for ReS<sub>2</sub> of monolayer, few layer (3 nm) and bulk, respectively. The observed 15 vibrational modes in the 100–400 cm<sup>−1</sup> range are associated with fundamental Raman modes (A<sub>1g</sub>, E<sub>2g</sub>, and E<sub>1g</sub>) coupled to each other and to acoustic phonons, which is significantly different from TMDs with higher hexagonal symmetries,<sup>[29,30]</sup> indicating the structure anisotropy of ReS<sub>2</sub>. The main peaks at 150 and 210.5 cm<sup>−1</sup> are corresponding to

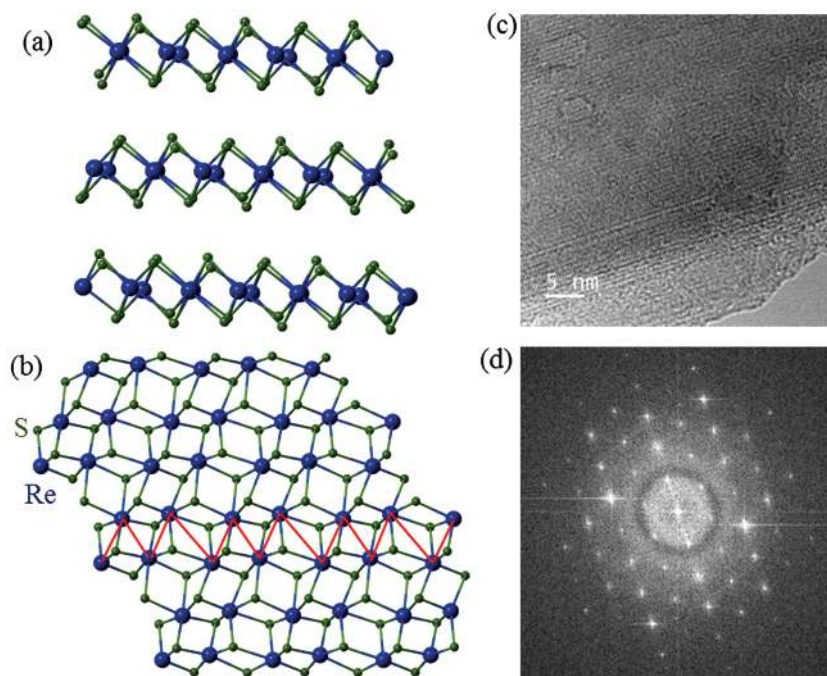


**Figure 1.** Crystal structure and TEM characteristics of the ReS<sub>2</sub>. a) Side view and b) top view of the crystal structure. The structure shows distorted 1T structure and Re-chain along the *b*-axis, as indicated by the red lines. c) The HRTEM and d) corresponding FFT pattern of ReS<sub>2</sub>, indicating the high crystalline of the exfoliated sample.

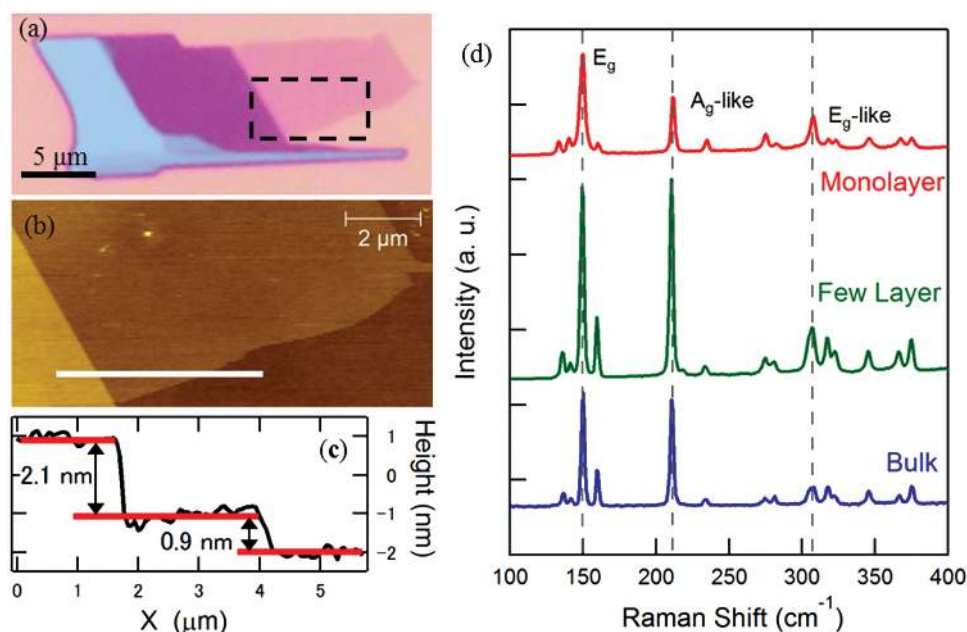


**Figure 2.** AFM and Raman characteristics of the  $\text{ReS}_2$ . a) Optical image of a typical  $\text{ReS}_2$  flake. Scale bar is 5  $\mu\text{m}$ . b) An AFM image of the area surrounded by black dashed lines in (a). c) The line profile of the  $\text{ReS}_2$  flake along the white line indicated in (b), showing a single-layer thickness of 0.9 nm for the monolayer range, and a thickness of 3 nm for the few layer range. d) The Raman spectrum of bulk (blue), few layer (green) and monolayer (red)  $\text{ReS}_2$ , respectively. The main peaks at 150  $\text{cm}^{-1}$  and 210.5  $\text{cm}^{-1}$  are corresponding to the in-plane ( $E_{2g}$ ) and mostly out-of-plane ( $A_{1g}$ -like) vibration modes, respectively. The Raman peaks are quite similar in the bulk, few-layer and monolayer forms, indicating weak interlayer coupling.

the in-plane ( $E_{2g}$ ) and mostly out-of-plane ( $A_{1g}$ -like) vibration modes, respectively. The peak positions are slightly different from the reported one, which is due to the differences of excitation laser wavelengths of 488 nm in the literature and 532 nm in this study.<sup>[31]</sup> When the thickness is thinned down to monolayer, the main Raman peaks show very small change due to weak interlayer coupling in  $\text{ReS}_2$ , which is consistent with previous report.<sup>[23]</sup>

In TMDs with perfect in-plane hexagonal lattice, different M points in the Brillouin zone (e.g., M1 and M2 in Figure 3a) are equivalent due to the sixfold symmetry. Therefore, the electronic dispersion along  $\Gamma$ -M1 and  $\Gamma$ -M2 should be identical. However, this case changes when lattice distortion takes place in  $\text{ReS}_2$ , which breaks the original symmetry and makes M1 and M2 inequivalent. Angle-resolved photoemission spectroscopy (ARPES) measurements have been carried out to study the electronic band dispersion along  $\Gamma$ -M1 and  $\Gamma$ -M2, respectively. Energy distribution curves (EDC) 2nd derivative images have been used to enhance the electronic structures and plotted in Figure 3 b,c with their momentum locations shown in Figure 3a. Clear differences can be recognized between the dispersion along  $\Gamma$ -M1 and  $\Gamma$ -M2, consistent with the theoretical calculations.<sup>[23]</sup>

The structure anisotropy is always associated with the optical and electrical property

anisotropies. In order to examine the in-plane optical anisotropy, we measured the polarization dependence of the absorption spectrum for cleaved  $\text{ReS}_2$  thin flake on a quartz substrate using the microscopic spectrophotometer. Inset of Figure 4a shows the optical image and orientation indication of crystal used for the measurement. Large anisotropy of absorption is observed by changing the polarization angle from 0° to 90° (with respect to the  $b$ -axis). Surprisingly the anisotropy is

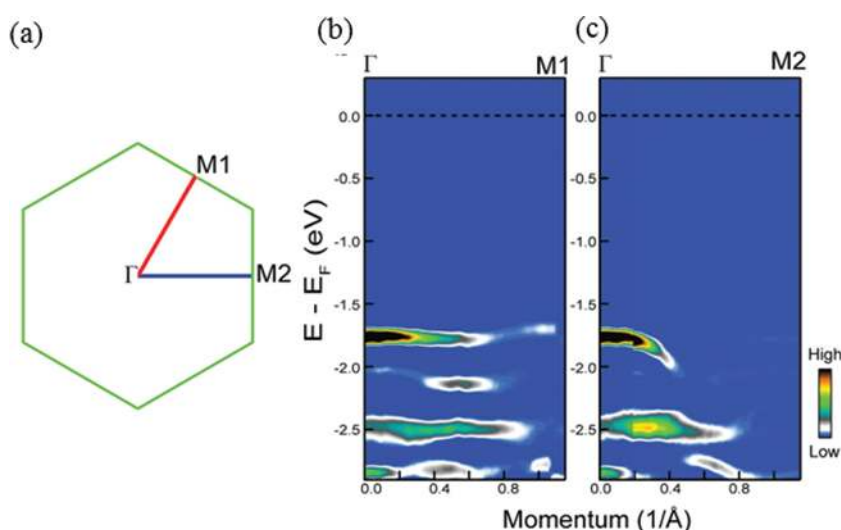


**Figure 3.** Anisotropic electronic structure of  $\text{ReS}_2$ . a) Undistorted hexagonal Brillouin zone of  $\text{ReS}_2$ . The band dispersion along  $\Gamma$ -M1 b) and  $\Gamma$ -M2 c) with their momentum locations marked in a. The differences between b and c indicate that the sixfold symmetry of the hexagonal Brillouin zone is broken due to lattice distortion.



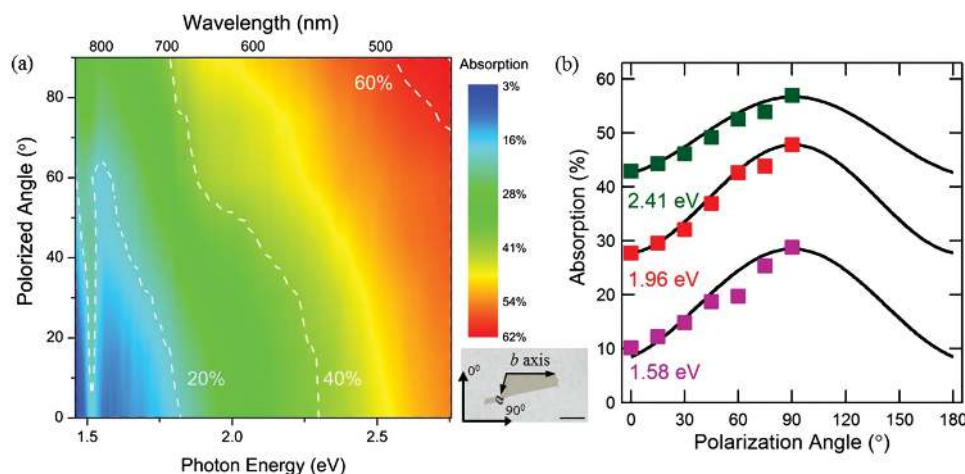


**Figure 4.** The polarization dependent absorption spectrum of atomically thin ReS<sub>2</sub>. a) 2D plot of absorption spectrum as a function of the polarization angle respect to the *b*-axis of the crystal structure. Inset of (a) shows the optical image of the ReS<sub>2</sub> with a thickness of about 12 nm. The definition of angle respect to the *b* axis is also shown, which will be used in the following measurement. Scale bar, 10 μm. b) Absorption as a function of polarization angle at different photo energies (2.41, 1.96, and 1.58 eV, respectively). They follow the sinusoidal function fitting (black line).

observed in a wide range from 1.55 eV (800 nm) to 2.76 eV (450 nm) (Figure 4a), which is different from previous reports in bulk samples, in which anisotropy is only observed in a small range around the band edge,<sup>[32,33]</sup> this probably originates from the enhanced transmission of light for the ultrathin ReS<sub>2</sub> layer. The broadband anisotropic absorption re-ignites interests for the study of polarization sensitive photodetector used in the visible to near infrared spectrum. Figure 4b plotted the absorption as a function of the polarization angle. The curve can be fitted with a sinusoidal function, which is identical to the band-edge absorption and Raman spectra spectrum change in anisotropic materials.<sup>[32,34]</sup> This in-plane anisotropy of ReS<sub>2</sub> is attributed to the field-induced polarization of the lattice, which leads to displacements of the lattice atoms, and consequently affects the electronic states of the solids.<sup>[35]</sup> The peak observed near band edge is related to the exciton absorption,<sup>[36]</sup> which is also polarization dependent, shifting from 1.51 to 1.48 eV by rotating the polarization from perpendicular to parallel *b*-axis direction (see the inset in Figure 4a). This polarization dependence of exciton absorption can be used for the wavelength and polarization sensitive luminescent applications.

### 3. Electronic Transport and Photoresonance Properties of ReS<sub>2</sub> Transistor

Electronic properties have a pronounced effect on the performance of photodetection. Before examining the photodetector performance, we first fabricated the field effect transistors (FETs) using atomically thin ReS<sub>2</sub> and studied their transport performances. The transistor was fabricated using the photolithography, following the deposition of Cr/Au (5/50 nm) electrodes using the high vacuum thermal evaporator. In order to study the polarization dependence of ReS<sub>2</sub> FET later, the conduction channels were made along the *b*-axis direction. **Figure 5a** shows the output characteristics of the device based on the flake with a thickness of about 3 nm, indicating an obvious

n-type semiconducting behavior of ReS<sub>2</sub>. The linear  $I_d$ - $V_d$  curve under low drain voltage indicates negligible Schottky barrier at the ReS<sub>2</sub> and Cr/Au interfaces. When the gate voltage was varied from -30 to 30 V while applying 0.1 V drain voltage, as shown in Figure 5b, the channel switched from off state to on state and an increase in drain current by a factor of 10<sup>5</sup> was observed. The measured on/off ratio is four orders of magnitude larger than those in graphene and comparable to the value recently reported in MoS<sub>2</sub> device.<sup>[37]</sup> The field-effect mobility was estimated from the linear region in the  $I_d$ - $V_g$  curve ( $V_g$  from 10 to 30 V) by using the equation  $\mu = \frac{dI_d}{dV_g} \times \frac{L}{WC_iV_d}$ , where  $L$  is the channel length,  $W$  is the channel width, and  $C_i$  is the capacitance between the channel and the back gate per unit area ( $C_i = \epsilon_0\epsilon_r/d$ ;  $\epsilon_0$  is the vacuum permittivity,  $\epsilon_r$  is the relative permittivity, and  $d$  is the thickness of SiO<sub>2</sub> layer), respectively. The mobility is calculated to be around 18 cm<sup>2</sup> V<sup>-1</sup> s<sup>-1</sup>, with  $L = 6.2$  μm,  $W = 1.7$  μm, and  $d = 285$  nm. This value is comparable to the values from exfoliated MoS<sub>2</sub> layers. Further improvement of the mobility will be achieved by optimizing the contact metals, the interface between the channel and gate dielectric or using high-*k* gate dielectric screening.<sup>[37–39]</sup>

To understand the mechanisms of limiting the mobility in ReS<sub>2</sub>, we examined the temperature dependence of the mobility from room temperature to 100 K (Figure 5c,d). By decreasing the temperature, the mobility increased monotonically to 40 cm<sup>2</sup> V<sup>-1</sup> s<sup>-1</sup>, due to the weak electron-phonon scattering at low temperature.<sup>[40]</sup> As shown in the inset of Figure 5d, the temperature dependence can be fitted by the power law  $\mu \propto T^{-\gamma}$ , where the exponent  $\gamma$  is about 1.1, which depends on the dominant phonon scattering mechanism. This value is same as that reported for bilayer MoS<sub>2</sub>,<sup>[41]</sup> and is smaller than that of monolayer MoS<sub>2</sub> and theoretical calculation.<sup>[40,42]</sup> Although some variations in the apparent phonon damping factor may be explained by charged impurity scattering and homopolar phonon quenching,<sup>[41]</sup> the origin of the observed  $\gamma$  in our work is still unclear, more experimental and theoretical calculation,

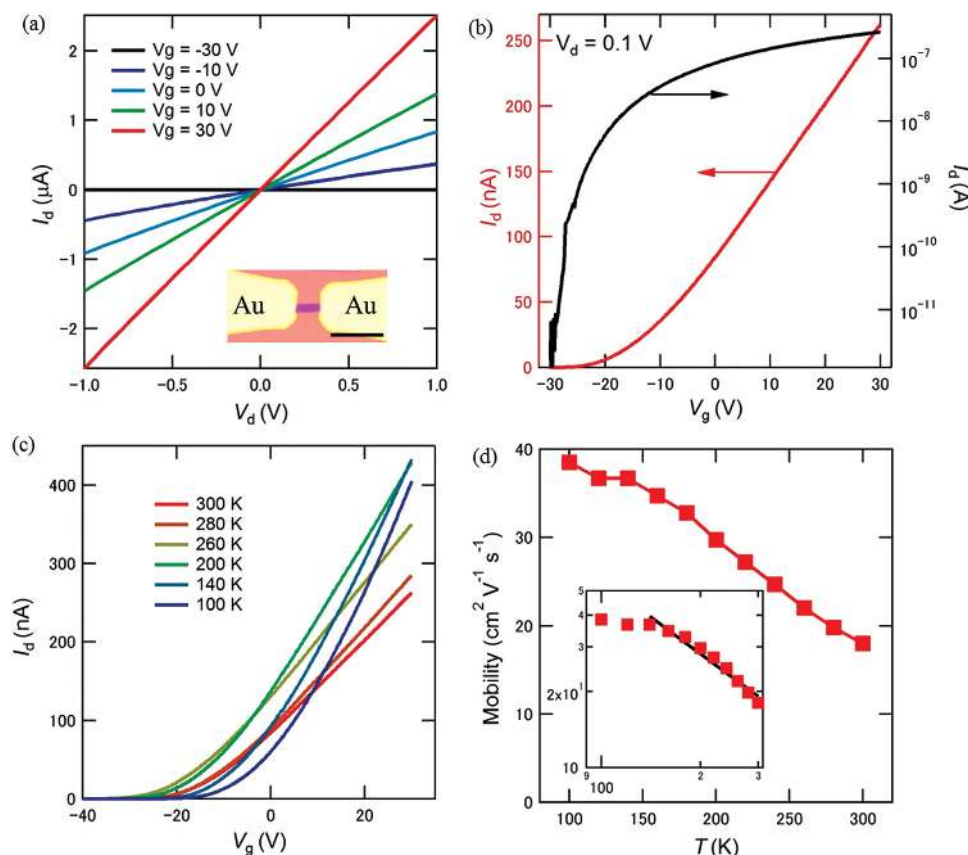


**Figure 5.** Characterization of the few layer  $\text{ReS}_2$  field effect transistor. a) Output transfer curve of the transistor at room temperature based on  $\text{ReS}_2$  with a thickness of about 3 nm. The transistor exhibits n-type behavior and low contact resistance. The inset shows a typical optical image of the transistor. Scale bar, 10  $\mu\text{m}$ . b) The linear (red) and log (black) scale plots of the transfer curve, showing a mobility of  $18 \text{ cm}^2 \text{ V}^{-1} \text{ s}^{-1}$  with a on/off ratio of about  $10^5$ . c) The  $I_d$ – $V_g$  transfer curve for the  $\text{ReS}_2$  transistor with a drain voltage of 0.1 V acquired at different temperatures. d) The field effect mobility as a function of temperature extracted from (c). The mobility increases gradually with decreasing temperature. The inset shows the power law fitting of the data, indicating the dominant electron-phonon scattering at higher temperature.

including much lower temperature measurement combining with the Hall mobility measurement, will be of much help for fully understanding the scattering mechanism and optimizing the device performance for  $\text{ReS}_2$  and other 2D materials.

The good electronic properties of  $\text{ReS}_2$  make it promising for the application of optoelectronic devices. In addition, the direct band gap nature of this material results in both a high absorption coefficient and efficient electron–hole pair generation under photoexcitation, which is crucial for high-performance photodetectors. We examined the photoresponse properties of atomically thin  $\text{ReS}_2$  ( $\approx 3 \text{ nm}$ ) in the two-terminal device geometry, using a typical green semiconductor laser (2.4 eV) as the illumination source (Figure 6a). The photoresponse under different wavelength excitations is also investigated and shown in Figure S1 (Supporting Information). The device shows good response to all the wavelength lights. Figure 6b shows the photocurrent as a function of drain bias. By increasing the light power the photocurrent becomes stronger. In Figure 6c, we have extracted the light power dependence of photocurrent at different drain voltages. It can clearly be seen that the photocurrent satisfies a simple power law relation  $I_{\text{ph}} \propto P^\alpha$ , where  $I_{\text{ph}}$  is the photocurrent,  $P$  is the light power, respectively. The index

of power law  $\alpha$  is deduced to be 0.3, which is attributed to complex processes in the carrier generation, trapping, and electron–hole recombination in the semiconductor.<sup>[43]</sup> The process for the photocurrent generation can be explained by a simplified energy band diagram (Figure 6d). The charge transfer via Fermi level tuning between the interface of metal electrodes and  $\text{ReS}_2$  channels, resulting in the band bending, and therefore forming Schottky type barriers as well as a depletion layers. Under the light illumination with the photon energy greater than the energy gap of the semiconductor, electron–hole pairs are excited by absorbing light and laterally separated by the applied drain bias, leading to the generation of photocurrent. The response of photodetector is proportional to the rate of incident beams of photons, which is consistent with the result in Figure 6c. The time dependent photoresponse of the  $\text{ReS}_2$  device carried out by mechanically modulating the intensity of the incoming light and recording the current change, and shown in Figure S2 (Supporting Information). Photoresponsivity  $R$ , as the ratio between the intensity of generated photocurrent to that of the incident light, is one of the most important parameters for a photodetector. Figure 6e shows the photoresponsivity evaluated at different bias voltages from Figure 6b, respectively. The

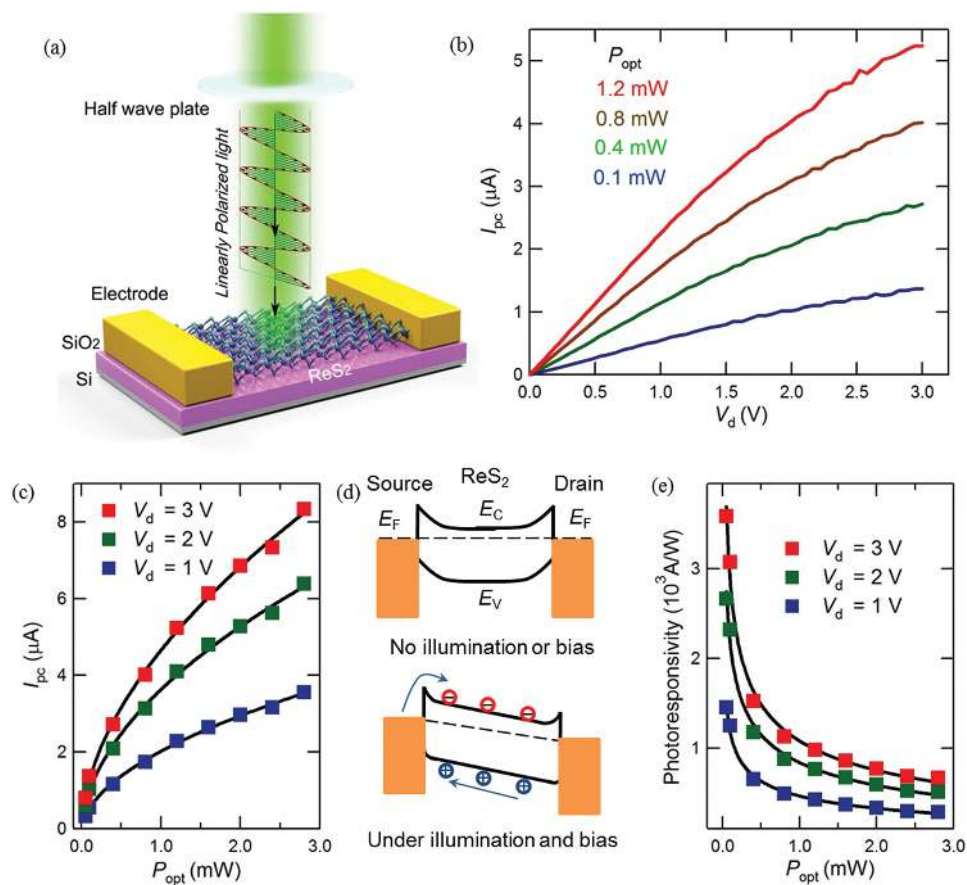


**Figure 6.** Photoresponse properties of the ReS<sub>2</sub> device. a) 3D schematic view of the photodetection device. The light is illuminated on the ReS<sub>2</sub> channel, and the light polarization is controlled by the half wave plate, which is used for the linear dichroism detection later. b) The photocurrent response as a function of drain voltage under different light intensity green light illumination. c) the photocurrent as a function of light intensity under a drain voltage of 1 V (blue), 2 V (green) and 3 V (red), respectively. The data can be fitted very well using the power law function (black line). d) Schematic band diagrams of the device under different illumination and bias conditions. E<sub>F</sub>, Fermi level; E<sub>C</sub>, Conduction band; E<sub>V</sub>, Valence band. The ReS<sub>2</sub> forms Schottky barriers with Cr/Au electrodes. When a light illuminates the device, electron–hole pairs are generated and separated by the applied drain voltage, generating photocurrents. e) The light intensity dependence of photoresponsivity deduced from (c) for drain voltages of 1 V (blue), 2 V (green), and 3 V (red), respectively. The black lines are guides to eyes.

device achieved a photoresponsivity of  $10^3 \text{ A W}^{-1}$  at low intensity of light. This value is several orders of magnitude higher than that of graphene-based photodetectors.<sup>[44]</sup> It is also comparable with the highest value of MoS<sub>2</sub>-based photodetectors,<sup>[45]</sup> and is three orders of magnitude higher than that of black phosphorus.<sup>[46]</sup> A sub-linear dependence of the photoresponse was observed upon tuning the light power. The presence of the trap states either in the channel or at the interface between ReS<sub>2</sub> and the underlying SiO<sub>2</sub> layer may be responsible for the reduction of the photoresponsivity at higher light power.<sup>[45]</sup>

The structure anisotropy induced linear dichroism in ReS<sub>2</sub> enables us to study the polarization sensitive photodetector. We now focus our study on the polarization sensitive detection of the device. The polarization of the illuminated light is controlled via the combination of one half wave plate and a polarizer. **Figure 7a** shows the evolution of photocurrent as a function of the polarization angle of the linear polarizer. By rotating the polarization of the light while keeping the incident power constant, the photocurrent changes dramatically. The

photocurrent with the incident light polarized along the *b*-axis (defined as 90° see inset of Figure 4a) is much stronger than that perpendicular to the *b*-axis (defined as 0°). This is a strong evidence that demonstrates the polarization dependent absorption and resulting photocurrent detection via linear dichroism. The photocurrents under drain voltages of 1, 2, and 3 V as a function of incident light polarization angle are shown in Figure 7b. The data can be perfectly fitted by a sinusoidal function. In addition, the photocurrent and absorption has a quite similar dependence on the incident light polarization, as shown in Figure 7c, which are plotted in the same polar coordination. This strongly suggests that the intrinsic polarization dependent photoresponse originates from ReS<sub>2</sub> itself. These observations clearly indicate that the incident light in different polarization states passing through the anisotropic ReS<sub>2</sub> experiences a varying absorption, directly reflecting the intrinsically anisotropic nature of the crystal structure. Due to the varying absorption in the wide wavelength range seen from the absorption spectrum, the polarization sensitive photodetection can be extended

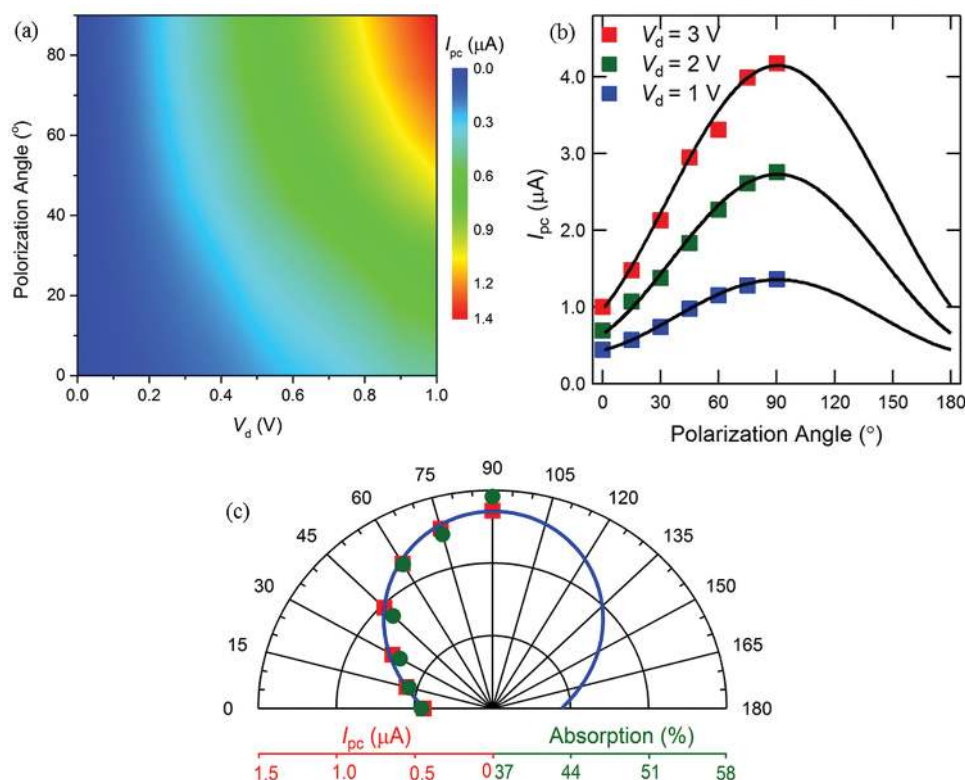


**Figure 7.** Polarization sensitive photoresponse of ReS<sub>2</sub>. a) The photocurrent change as a function of drain bias under different polarization light illuminations. b) The change of the photocurrent under different drain biases plotted as a function of polarization angle, the data can be fitted very well using a power law function (black line). c) The photocurrent with drain bias of 1 V (red square) and absorption (green circle) measured under different polarization angle of green light and plotted in polar coordinates. The blue lines are the fitting results using sinusoidal function. The consistence between photocurrent and absorption indicates the intrinsic linear dichroic response of ReS<sub>2</sub>.

to a wide range from visible to near infrared. Compared to the reported polarization sensitive device based on a wire-grid polarizer relying on nanofabrication processes,<sup>[26]</sup> our demonstrations prove that atomically thin ReS<sub>2</sub> can be used as a potential intrinsic linear dichroism media with high responsivity for practical integrated optical applications.

## 4. Conclusions

In this work, we have studied the electronic and photoresponse properties of atomically thin ReS<sub>2</sub> obtained by mechanical exfoliation method. The electron mobility up to  $40 \text{ cm}^2 \text{ V}^{-1} \text{ s}^{-1}$  was obtained with an on/off ratio of about  $10^5$ . The device also shows a good photoresponse with a photoresponsivity of  $10^3 \text{ A W}^{-1}$ . The linear dichroic photodetector based on anisotropic ReS<sub>2</sub> is demonstrated, which is ascribed to the polarization sensitive absorption induced by crystal structure anisotropy. Combining with the environmental stability and unique physical properties like weak interlayer coupling of ReS<sub>2</sub>, together with the high flexibility of 2D materials,<sup>[47]</sup> the linear dichroism observed in ReS<sub>2</sub> leads to a new degree of freedom to manipulate electronic and optoelectronic properties and opens up exciting opportunities of novel integrated optical and optoelectronic device applications for polarization detection. The advantage of the simple

transistor architecture reported here allows the polarization dependent phototransistor to be used as part of a circuit, for example, as part of a complementary inverter or ring oscillator. Recent progress in growth of 2D materials and heterostructure,<sup>[48–50]</sup> should allow the creation of arrays of micrometre-scale devices, as well as integration with CMOS electronics and ultimate thin light polarization detection devices based on anisotropic ReS<sub>2</sub> and other 2D materials.<sup>[45,51]</sup>

## 5. Experimental Section

**Isolation and Characterization of ReS<sub>2</sub> Flake:** The ReS<sub>2</sub> single crystals were synthesized through chemical vapor transport using iodine as the transport agent. A scotch-tape method was used to exfoliate ReS<sub>2</sub> flakes on the degenerately doped Si substrate covered with 285 nm SiO<sub>2</sub>. Optical identification was conducted with Olympus BX51 microscope. Thickness of the thin flake was measured by Asylum Research Cypher S Atomic Force Microscopy (AFM) in trapping mode. Raman spectrum characterization was performed using Witec confocal Raman system under 532 nm laser excitation. HRTEM image was obtained using FEI Tecnai F20 system. The ARPES experiments were carried out at Beamline 5–4 of the Stanford Synchrotron Radiation Lightsource (SSRL) of Slac National Accelerator Laboratory using 25 eV photons with a base pressure better than  $5 \times 10^{-11}$  Torr. Absorption spectrum was characterized by Jasco MSV-5200 microscopic spectrophotometer.



**Device Fabrication and Measurement:** The electrodes were patterned via photolithography, followed by thermal evaporation of Cr/Au (5/50 nm) and subsequent lift-off process. Electric characterization was performed by using the Agilent B1500 semiconductor parameter analyzer. Low temperature measurement was performed in a probe station cooled by liquid nitrogen. The photoresponse was measured using a semiconductor green laser as the illumination source, in the ambient condition. Light power dependence of the photoresponse was performed by tuning the light power while keeping the light polarization unchanged. Polarization dependence of the photoresponse was carried out by rotating the polarization of the light using a half wave plate and a polarizer, while keeping the light power unchanged throughout the measurement.

## Supporting Information

Supporting Information is available from the Wiley Online Library or from the author.

## Acknowledgements

F.L. and S.Z. contributed equally to this work. The authors acknowledge Zhen Fei and Chuanhong Jin from the Center for Electron Microscopy Zhejiang University China for the help on the HRTEM characterization. This work was supported by the Singapore National Research Foundation under NRF RF Award No. NRF-RF2013-08, the start-up funding from Nanyang Technological University (M4081137.070) and MOE Tier 1 grant RG10/14. H.J.F. thanks the support from the Ministry of Education of Singapore (Grant No. MOE2011-T3-1-005). T.R.M. acknowledges the support by NSF Fellowship (NSF GRFP DGE-1258923). L.S. thanks the support from National Natural Science Foundation of China (U1232131, U1532112, 11375198, 11574280) and Prof. Zhe Sun at Hefei Synchrotron Radiation Facility (NSRL) for helps in the ARPES characterization. W.L.C., X.W. and B.K.T. thank the support from NTU-A\*STAR Silicon Technologies Centre for Excellence under the program Grant No. 11235100003.

Received: October 23, 2015

Revised: November 14, 2015

Published online:

- [1] J. S. Tyo, D. L. Goldstein, D. B. Chenault, J. A. Shaw, *Appl. Opt.* **2006**, 45, 5453.
- [2] C. Chen, K. Choi, L. Rokhsinon, W. Chang, D. Tsui, *Appl. Phys. Lett.* **1999**, 74, 862.
- [3] J. Wang, M. S. Gudiksen, X. Duan, Y. Cui, C. M. Lieber, *Science* **2001**, 293, 1455.
- [4] X. He, X. Wang, S. Nanot, K. Cong, Q. Jiang, A. A. Kane, J. E. Goldsmith, R. H. Hauge, F. Léonard, J. Kono, *ACS Nano* **2013**, 7, 7271.
- [5] Q. H. Wang, K. Kalantar-Zadeh, A. Kis, J. N. Coleman, M. S. Strano, *Nat. Nanotechnol.* **2012**, 7, 699.
- [6] F. Koppens, T. Mueller, P. Avouris, A. Ferrari, M. Vitiello, M. Polini, *Nat. Nanotechnol.* **2014**, 9, 780.
- [7] M. Chhowalla, H. S. Shin, G. Eda, L.-J. Li, K. P. Loh, H. Zhang, *Nat. Chem.* **2013**, 5, 263.
- [8] G. Fiori, F. Bonaccorso, G. Iannaccone, T. Palacios, D. Neumaier, A. Seabaugh, S. K. Banerjee, L. Colombo, *Nat. Nanotechnol.* **2014**, 9, 768.
- [9] F. Xia, H. Wang, D. Xiao, M. Dubey, A. Ramasubramaniam, *Nat. Photonics* **2014**, 8, 899.
- [10] K. Novoselov, A. K. Geim, S. Morozov, D. Jiang, M. K. I. Grigorieva, S. Dubonos, A. Firsov, *Nature* **2005**, 438, 197.
- [11] K. S. Novoselov, Z. Jiang, Y. Zhang, S. Morozov, H. Stormer, U. Zeitler, J. Maan, G. Boebinger, P. Kim, A. Geim, *Science* **2007**, 315, 1379.
- [12] Y. Zhang, Y.-W. Tan, H. L. Stormer, P. Kim, *Nature* **2005**, 438, 201.
- [13] A. Chernikov, T. C. Berkelbach, H. M. Hill, A. Rigosi, Y. Li, O. B. Aslan, D. R. Reichman, M. S. Hybertsen, T. F. Heinz, *Phys. Rev. Lett.* **2014**, 113, 076802.
- [14] K. F. Mak, K. He, J. Shan, T. F. Heinz, *Nat. Nanotechnol.* **2012**, 7, 494.
- [15] K. F. Mak, C. Lee, J. Hone, J. Shan, T. F. Heinz, *Phys. Rev. Lett.* **2010**, 105, 136805.
- [16] H. Zeng, J. Dai, W. Yao, D. Xiao, X. Cui, *Nat. Nanotechnol.* **2012**, 7, 490.
- [17] Z. Ye, T. Cao, K. O'Brien, H. Zhu, X. Yin, Y. Wang, S. G. Louie, X. Zhang, *Nature* **2014**, 513, 214.
- [18] T. Hong, B. Chamlagain, W. Lin, H.-J. Chuang, M. Pan, Z. Zhou, Y.-Q. Xu, *Nanoscale* **2014**, 6, 8978.
- [19] F. N. Xia, H. Wang, Y. C. Jia, *Nat. Commun.* **2014**, 5, 4458.
- [20] H. Yuan, X. Liu, F. F. Afshinmanesh, W. Li, G. Xu, J. Sun, B. Lian, A. G. Curto, G. Ye, Y. Hikita, Z. Shen, S.-C. Zhang, X. Chen, M. Brongersma, H. Y. Hwang, Y. Cui, *Nat. Nanotechnol.* **2015**, 10, 707.
- [21] J. Wilson, A. Yoffe, *Adv. Phys.* **1969**, 18, 193.
- [22] Y. Feng, W. Zhou, Y. Wang, J. Zhou, E. Liu, Y. Fu, Z. Ni, X. Wu, H. Yuan, F. Miao, B. Wang, X. Wan, D. Xing, *Phys. Rev. B* **2015**, 92, 054110.
- [23] S. Tongay, H. Sahin, C. Ko, A. Luce, W. Fan, K. Liu, J. Zhou, Y.-S. Huang, C.-H. Ho, J. Yan, D. F. Ogletree, S. Aloni, J. Ji, S. Li, J. Li, F. M. Peeters, J. Wu, *Nat. Commun.* **2014**, 5, 3252.
- [24] E. Liu, Y. Fu, Y. Wang, Y. Feng, H. Liu, X. Wan, W. Zhou, B. Wang, L. Shao, C.-H. Ho, Y.-S. Huang, Z. Cao, L. Wang, A. Li, J. Zeng, F. Song, X. Wang, Y. Shi, H. Yuan, H. Y. Hwang, Y. Cui, F. Miao, D. Xing, *Nat. Commun.* **2014**, 6, 6991.
- [25] Q. Cui, H. Zhao, *ACS Nano* **2015**, 9, 3935.
- [26] S. Ura, H. Sunagawa, T. Suhara, H. Nishihara, *J. Lightwave Technol.* **1988**, 6, 1028.
- [27] H. Murray, S. Kely, R. Chianelli, C. Day, *Inorg. Chem.* **1994**, 33, 4418.
- [28] K. Novoselov, D. Jiang, F. Schedin, T. Booth, V. Khotkevich, S. Morozov, A. Geim, *Proc. Natl. Acad. Sci. USA* **2005**, 102, 10451.
- [29] A. Berkdemir, H. R. Gutierrez, A. R. Botello-Mendez, N. Perea-Lopez, A. L. Elias, C.-I. Chia, B. Wang, V. H. Crespi, F. Lopez-Urisa, J.-C. Charlier, H. Torronces, M. Terrones, *Sci. Rep.* **2013**, 3, 1755.
- [30] H. Li, Q. Zhang, C. C. R. Yap, B. K. Tay, T. H. Tong, A. Olivier, D. Baillargeat, *Adv. Funct. Mater.* **2012**, 22, 1385.
- [31] T. Fujita, Y. Ito, Y. Tan, H. Yamaguchi, D. Hojo, A. Hirata, D. Voiry, M. Chhowalla, M. Chen, *Nanoscale* **2014**, 6, 12458.
- [32] C. Ho, Y. Huang, K. Tiong, P. Liao, *J. Phys. Condens. Matter.* **1999**, 11, 5367.
- [33] G. Dresselhaus, *Phys. Rev.* **1957**, 105, 135.
- [34] S. Zhang, J. Yang, R. Xu, F. Wang, W. Li, M. Ghufan, Y.-W. Zhang, Z. Yu, G. Zhang, Q. Qin, Y. Lu, *ACS Nano* **2014**, 8, 9590.
- [35] G. Weiser, *Surf. Sci.* **1973**, 37, 175.
- [36] C. Ho, P. Liao, Y. Huang, K. Tiong, *Phys. Rev. B* **1997**, 55, 15608.
- [37] B. Radisavljevic, A. Radenovic, J. Brivio, V. Giacometti, A. Kis, *Nat. Nanotechnol.* **2011**, 6, 147.
- [38] W. Liu, J. Kang, D. Sarkar, Y. Khatami, D. Jena, K. Banerjee, *Nano Lett.* **2013**, 13, 1983.
- [39] B. Chamlagain, Q. Li, N. J. Ghimire, H.-J. Chuang, M. M. Perera, H. Tu, Y. Xu, M. Pan, D. Xiao, J. Yan, *ACS Nano* **2014**, 8, 5079.
- [40] B. Radisavljevic, A. Kis, *Nat. Mater.* **2013**, 12, 815.
- [41] B. W. Baugher, H. O. Churchill, Y. Yang, P. Jarillo-Herrero, *Nano Lett.* **2013**, 13, 4212.



- [42] K. Kaasbjerg, K. S. Thygesen, K. W. Jacobsen, *Phys. Rev. B* **2012**, *85*, 115317.
- [43] H. Kind, H. Yan, B. Messer, M. Law, P. Yang, *Adv. Mater.* **2002**, *14*, 158.
- [44] T. Mueller, F. Xia, P. Avouris, *Nat. Photonics* **2010**, *4*, 297.
- [45] O. Lopez-Sanchez, D. Lembke, M. Kayci, A. Radenovic, A. Kis, *Nat. Nanotechnol.* **2013**, *8*, 497.
- [46] N. Youngblood, C. Chen, S. J. Koester, M. Li, *Nat. Photon.* **2015**, *9*, 247.
- [47] D. Akinwande, N. Petrone, J. Hone, *Nat. Commun.* **2014**, *5*, 5678.
- [48] G. H. Han, N. J. Kybert, C. H. Naylor, B. S. Lee, J. Ping, J. H. Park, J. Kang, S. Y. Lee, Y. H. Lee, R. Agarwal, A. T. Charlie Johnson, *Nat. Commun.* **2015**, *6*, 6128.
- [49] Z. Liu, L. Ma, G. Shi, W. Zhou, Y. Gong, S. Lei, X. Yang, J. Zhang, J. Yu, K. P. Hackenberg, A. Babakhani, J.-C. Idrobo, R. Vajtai, J. Lou, P. M. Ajayan, *Nat. Nanotechnol.* **2013**, *8*, 119.
- [50] Z. Kang, S. Xie, L. Huang, Y. Han, P. Y. Huang, K. F. Mak, C. Kim, D. Muller, J. Park, *Nature* **2015**, *520*, 656.
- [51] H.-M. Li, D. Lee, D. Qu, X. Liu, J. Ryu, A. Seabaugh, W. J. Yoo, *Nat. Commun.* **2015**, *6*, 6564.